# Five-Level Active-Neutral-Point-Clamped DC/DC Converter for Medium-Voltage DC Grids

Liu, Dong; Deng, Fujin; Chen, Zhe

*Published in:*
I E E E Transactions on Power Electronics

*DOI (link to publication from Publisher):*
10.1109/TPEL.2016.2585618

*Publication date:*
2017

*Document Version*
Accepted author manuscript, peer reviewed version

# Five-Level Active-Neutral-Point-Clamped DC/DC Converter for Medium Voltage DC Grids

Dong Liu, *Student Member, IEEE*, Fujin Deng, *Member, IEEE*, and Zhe Chen, *Senior Member, IEEE*

***Abstract*—This paper proposes a five-level active-neutral-point-clamped (5L-ANPC) dc/dc converter for applications in medium voltage dc (MVDC) grids. A modulation strategy is proposed for the 5L-ANPC dc/dc converter to generate multi-level voltage waveforms, which can effectively reduce voltage change rate *dv/dt*, reduce voltage stress on the transformer, and thus reduce the electromagnetic interference (EMI) and increase reliability. An elimination method for the dead time effect is also proposed along with the proposed modulation strategy by employing a switch in series with the flying capacitor, which can effectively eliminate high voltage leaps caused by the dead time effect. In addition, a capacitor voltage control strategy is proposed for the 5L-ANPC dc/dc converter to ensure the balanced flying capacitor voltage and desired five-level voltage waveforms. Finally, simulation and experimental studies are conducted, and the results have verified the proposed converter and control strategies.**

***Index Terms*—Dc/dc converter, five-level active-neutral-point-clamped (5L-ANPC), medium voltage dc (MVDC) grids.**

## I. Introduction

DC-based distributions and dc-based micro-grids have been proposed as promising solutions for future smart-grid systems because of their clear merits, such as no reactive power, no frequency stability, high conversion efficiency, and easy system control [1-3]. Furthermore, dc-based data centers and residential systems have also been increasingly developed recently [4], [5]. The performance of dc-based systems highly depends on dc/dc converters because these converters are responsible for delivering power and changing voltage levels among dc-based systems. Accordingly, a dc/dc converter with high performances and high reliability is desired for the dc grids.

So far, a number of dc/dc converters for dc grids have been reported in literature and these dc/dc converters can be classified into two types, namely non-isolated converters and isolated converters. The isolated converters can gain galvanic isolation and a high ratio of voltage conversion by utilizing the high frequency transformer in comparison with the non-isolated converters [6], [7], and thus increase the reliability and safety of whole dc-based systems [8], [9], which makes them normally applied into the medium voltage dc-based systems [10-13]. Generally, there are mainly three types of isolated dc/dc converters including two-level based isolated converters, three-level (TL) based isolated converters, and modular multilevel converters (MMC). The two-level based isolated dc/dc converters require least quantity of power switches in medium voltage applications [11-13]. However, the power switches in them have to withstand the full dc bus voltage, which results in high conduction losses, high voltage change rate *dv*/*dt*, and large electromagnetic interference (EMI) [14-16]. The MMC distinguish themselves from others due to their low switches' voltage stress, low EMI, and good power quality arising from the increasing amount of voltage levels [17-19]. However, it would require more power switches, voltage transducers with increased cost [20], and complicated control algorithm for capacitor voltage balancing [21], [22]. Normally, the two-level based converters and MMC are more suitable for power transmission in low voltage and high voltage dc-based distributions [23], [24] respectively.

The TL based isolated dc/dc converters were presented in [25-35] with the advantage of low switch voltage stress, good EMI, improved power quality, and small filter size in comparison with the two-level based isolated dc/dc converter, simpler circuit structure, easier control strategy, and more reliability in comparison with MMC. Therefore, TL based converters are regarded as a favorable choice for high power converters applied to the medium voltage dc (MVDC) grids [25] with dc bus voltage of several thousand volts [36-38]. In 1992, a novel TL dc/dc converter was first proposed to lower the switch voltage stress for high voltage applications [26]. A zero voltage and zero current switching TL dc/dc converter was proposed in [27], in which a flying capacitor in primary side and an auxiliary circuit in the secondary side are added to achieve zero voltage switching of the leading switches and zero current switching of the lagging switches for improving the converter's efficiency. The soft switching technique for the TL dc/dc converter was systematically discussed in [28]. An isolated full bridge TL (FBTL) dc/dc converter and a hybrid isolated FBTL dc/dc converter were presented in [29] and [30] respectively, in which a double phase-shift control strategy and a chopping phase-shift control strategy were proposed respectively to achieve soft switching in FBTL converter. Other research works about the TL based dc/dc converters have also been conducted on the topics of topology and control strategy [31-34]. The major contributions of above works are mainly

This work was supported by the China Scholarship Council and Department of Energy Technology, Aalborg University, Denmark.

Dong Liu, Fujin Deng, and Zhe Chen are with the Department of Energy Technology, Aalborg University, Aalborg, 9220 Denmark (dli@et.aau.dk, fde@et.aau.dk, zch@et.aau.dk).

focused on soft switching techniques and power density to increase the converter's efficiency. When it comes to the applications of MVDC grids, the voltage stress on the transformer in TL based converters should be taken into consideration since MVDC grids have a high dc bus voltage and such high dc bus voltage would increase the voltage stress on the transformer, thus increases EMI and decreases the system reliability. However, little attention has been put on this topic in literatures so far. An improved FBTL dc/dc converter with a voltage balance control strategy was proposed in [35] for wind turbines in medium voltage dc-based system, which can reduce the *dv/dt* and voltage stress on the transformer. However, a passive filter is added into the primary side of the transformer, which reduces the step-up rate and converter's efficiency.

In this paper, a 5L-ANPC dc/dc converter with the corresponding modulation strategy is proposed to step down the medium voltage about several thousands volts to the low voltage about a few hundred volts [39-41] for the dc loads, which can effectively reduce voltage change rate *dv*/*dt*, reduce voltage stress on the transformer, thus reduce EMI and increase reliability. Comparing with the FBTL dc/dc converter, the proposed converter makes the power switches with low voltage stress ($V_{in}$/4) applicable to generate the five-level voltages. A switch in series with the flying capacitor is employed in the proposed dc/dc converter structure, which can effectively eliminate the dead time effect along with the proposed modulation strategy. In addition, a capacitor voltage control strategy is proposed to balance the voltage of the flying capacitor, which can ensure the generation of desired multi-level voltage waveforms. The proposed converter is inspired by the conventional 5L-ANPC inverter [42], [43]. However, the proposed voltage control strategy of the flying capacitor and elimination method for the dead time effect mentioned above are original improvements for the 5L-ANPC dc/dc converter. Finally, the proposed converter and capacitor voltage control strategy is validated by simulation as well as experimentation with a down-scale laboratory prototype.

This paper is organized as follows. Section II introduces the structure and modulation strategy of the proposed converter. The dead time effect on the proposed converter and its elimination method are discussed in section III. In section IV, a capacitor voltage control strategy is proposed for balancing the flying capacitor's voltage. Section V presents the simulation and experimentation results to verify the theoretical analysis. Finally, the main contributions of this paper are summarized in Section VI.

## II. Proposed 5L-ANPC DC/DC Converter

### A. Structure of Proposed Converter

Fig. 1 shows the structure of the proposed 5L-ANPC dc/dc converter. In the primary side, two input capacitors $C_1$, $C_2$ are used to split the input voltage $V_{in}$ into two voltages $V_{c1}$ and $V_{c2}$. $S_1$-$S_9$ and $D_1$-$D_9$ are power switches and power diodes. $C_3$ is the flying capacitor of the proposed converter. $T_r$ is the medium frequency transformer (MFT) to gain voltage level conversion and galvanic isolation. In the secondary side, there are four rectifier diodes $D_{r1}$-$D_{r4}$, an output filter inductor $L_o$, and an output filter capacitor $C_o$. $i_{c3}$ is the current flowing through the flying capacitor $C_3$. $i_{Lo}$ and $i_o$ are the currents flowing through output inductor $L_o$ and load respectively. $V_{c3}$ and $V_{out}$ are the voltage of $C_3$ and output. $V_{ab}$ and $i_p$ are the primary side voltage and current of MFT. The positive directions of currents $i_{c3}$, $i_p$, $i_{Lo}$, $i_o$ and voltages $V_{c1}$, $V_{c2}$, $V_{c3}$, $V_{ab}$, $V_{out}$ are defined as shown in Fig. 1. One thing to be mentioned is that $S_9$ is employed in series with the flying capacitor in order to eliminate the dead time effect, which will be analyzed in detail in Section III.

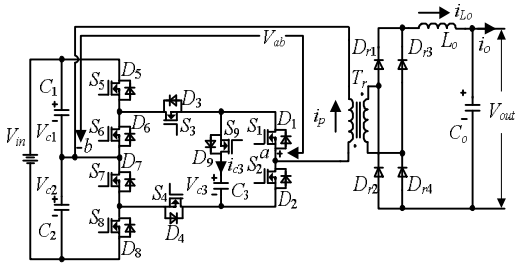


Fig. 1. Structure of the proposed 5L-ANPC dc/dc converter.

### B. Proposed Modulation Strategy

A modulation strategy including two operation modes with different switching sequences is proposed to generate five-level voltages on the primary of the transformer ($V_{ab}$) as shown in Fig. 2, in which ($S_1$, $S_2$), ($S_3$, $S_4$), ($S_5$, $S_6$), and ($S_7$, $S_8$) are complementary switch pairs; $d_{rv1}$-$d_{rv9}$ are driving signals for power switches $S_1$-$S_9$; $D_1$-$D_4$ are duty ratios in one cycle period, which are the same in the operation mode I and II; $T_s$ is the time period of one cycle. In the normal operation conditions, $V_{c1}$ = $V_{c2}$ = $V_{in}$/2 and $V_{c3}$ = $V_{in}$/4.

*1) Operation mode I:* Fig. 2(a) illustrates the operation mode I in one cycle. In the first half cycle, the driving signal $d_{rv1}$ lags behind $d_{rv3}$ by ($D_2$-$D_1$)×$T_s$/2. In the second half cycle, $d_{rv2}$ lags behind $d_{r4}$ by ($D_2$-$D_1$)×$T_s$/2. The duty ratios of $d_{rv5}$ and $d_{rv8}$ are both $D_3$ and less than 0.5, but $d_{rv8}$ delays $T_s$/2 from $d_{rv5}$. Similarly, the duty ratios of $d_{rv6}$ and $d_{rv7}$ are the same but more than 0.5 since ($d_{rv5}$, $d_{rv6}$) and ($d_{rv7}$, $d_{rv8}$) are complementary pairs respectively. Therefore, there is an overlap time $\Delta T_L$ between $d_{rv6}$ and $d_{rv7}$ in every half cycle as shown in Fig. 2. In the operation mode I, there are eight switching states namely $V0$, $V2$, $V3$, $V4$, $V5$, $V6$, $V7$, and $V9$ as listed in Table I. The flying capacitor is charged in switching states $V2$ and $V7$, which in turn means the current flowing through the flying capacitor $i_{c3}$ is positive in such two switching states as shown in Fig. 2(a).

*2) Operation mode II:* The operation mode II is similar to the operation mode I, which is shown in Fig. 2(b). The driving signal $d_{rv3}$ lags behind $d_{rv1}$ by ($D_2$-$D_1$)×$T_s$/2 in the first half cycle. In the second half cycle, $d_{rv4}$ lags behind $d_{rv2}$ by ($D_2$-$D_1$)×$T_s$/2. In the operation mode II, there are also eight switching states including $V1$, $V3$, $V4$, $V5$, $V6$, $V8$, and $V9$ as listed in Table I. In addition, the flying capacitor is discharged in switching states $V1$ and $V8$, which in turn means the current flowing through the flying capacitor $i_{c3}$ is negative in such two switching states as shown in Fig. 2(b).

Comparing the operation mode I with the operation mode II as shown in Fig. 2, it can be observed that: 1) the driving signals $d_{rv5}$, $d_{rv6}$, $d_{rv7}$, and $d_{rv8}$ are the same in the operation mode I and

II; 2) the driving signals $d_{rv1}$ and $d_{rv3}$ are shifted with each other between the operation mode I and II, which is the same for $d_{rv2}$ and $d_{rv4}$.

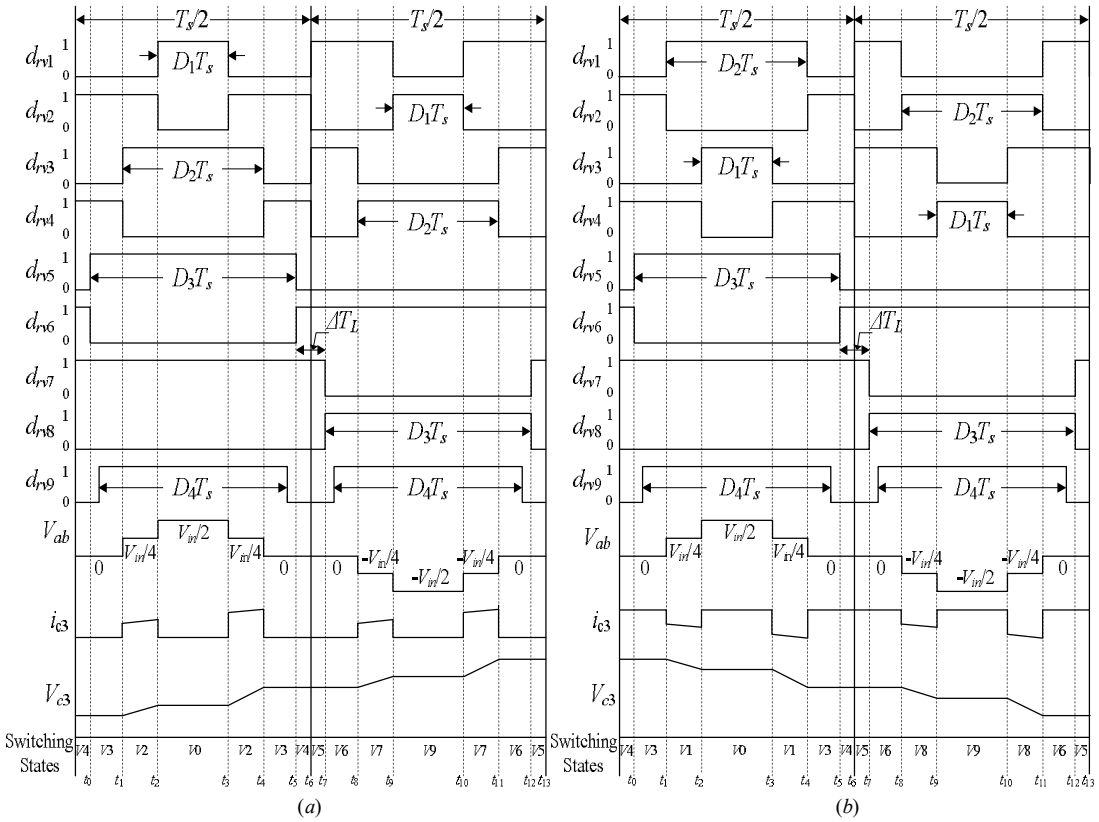


Fig. 2. Proposed modulation strategy. (a) Operation mode I. (b) Operation mode II.

TABLE I
SWITCHING STATES AND CIRCUIT OPERATION STATUSES OF THE 5L–ANPC CONVERTER

| Switching State | $S_1$ | $S_2$ | $S_3$ | $S_4$ | $S_5$ | $S_6$ | $S_7$ | $S_8$ | $S_9$ | $V_{ab}$ | $i_{c3}$ |
|---|---|---|---|---|---|---|---|---|---|---|---|
| $V0$ | 1 | 0 | 1 | 0 | 1 | 0 | 1 | 0 | 1 | $V_{c1}$ ($V_{in}$/2) | 0 |
| $V1$ | 1 | 0 | 0 | 1 | 1 | 0 | 1 | 0 | 1 | $V_{c3}$ ($V_{in}$/4) | -$\|i_p\|$ |
| $V2$ | 0 | 1 | 1 | 0 | 1 | 0 | 1 | 0 | 1 | $V_{c1}$-$V_{c3}$ ($V_{in}$/4) | +$\|i_p\|$ |
| $V3$ | 0 | 1 | 0 | 1 | 1 | 0 | 1 | 0 | 1 | 0 | 0 |
| $V4$ | 0 | 1 | 0 | 1 | 0 | 1 | 1 | 0 | 0 | 0 | 0 |
| $V5$ | 1 | 0 | 1 | 0 | 0 | 1 | 1 | 0 | 0 | 0 | 0 |
| $V6$ | 1 | 0 | 1 | 0 | 0 | 1 | 0 | 1 | 1 | 0 | 0 |
| $V7$ | 1 | 0 | 0 | 1 | 0 | 1 | 0 | 1 | 1 | -($V_{c2}$-$V_{c3}$) (-$V_{in}$/4) | +$\|i_p\|$ |
| $V8$ | 0 | 1 | 1 | 0 | 0 | 1 | 0 | 1 | 1 | -$V_{c3}$ (-$V_{in}$/4) | -$\|i_p\|$ |
| $V9$ | 0 | 1 | 0 | 1 | 0 | 1 | 0 | 1 | 1 | -$V_{c2}$ (-$V_{in}$/2) | 0 |

## III. Proposed Elimination Method For Dead Time Effect

In this section, an elimination method for the dead time effect by employing a power switch in series with the flying capacitor is proposed along with the proposed modulation strategy to eliminate the high voltage leaps caused by the dead time effect.

### *A. Analysis of Dead Time Effect*

In practical circuits, the dead time has to be set for each complementary switch pairs to avoid that they are switched on at the same time. For instance, if $S_5$ and $S_6$ are switched on simultaneously, the input capacitor $C_1$ will be shorted, which will damage $S_5$ and $S_6$ due to the overcurrent. In the operation mode I, if switch $S_9$ is not employed, the dead time $\Delta T_d$ between every two adjacent half cycles would lead a high voltage leap on the primary side voltage of MFT $V_{ab}$ as marked in Fig. 3. The reason of causing such high voltage leaps in the operation mode II is same as that in the operation mode I, so only operation mode I and its equivalent circuits are shown in Fig. 3 and Fig. 4 for explanation. Before analyzing such reason, two simplifications are made here: 1) all the power devices and diodes are ideal, which means rise time and fall time of the power switches and diodes are neglected and the switch junction capacitance effects on the circuit operation are

neglected; 2) the dead times are same for all complementary pairs.

Before $t_5$, $V_{ab}$ is 0 V because $S_2$, $S_4$, and $S_7$ are all in the on-state as shown in Fig. 4(a). At $t_5$, $S_2$, $S_4$, $S_5$, and $S_7$ are switched off simultaneously, and thus the transformer's primary current $i_p$ freewheels through $C_2$, $D_8$, $D_4$, and $D_2$ as shown in Fig. 4(b) (red area), which leads that $V_{ab}$ decreases to $-V_{c2}$ ($-V_{in}/2$) from 0 V. At $t_6$, $S_1$, $S_3$, $S_6$, and $S_8$ are switched on, $V_{ab}$ returns to 0 V with the connection of $S_1$, $S_3$, and $S_6$ as shown in Fig. 4(c). At $t_{11}$, $S_1$, $S_3$, $S_6$, and $S_8$ are switched off, which causes that $V_{ab}$ increases to $V_{c1}$ ($V_{in}/2$) from 0 V by the path connected through $D_1$, $D_3$, $D_5$, and $C_1$ as shown in Fig. 4(d). The analysis of following operation behaviors as shown in Fig. 3 (blue area) is similar to that in the last half cycle (red area in Fig. 3), which is not repeated here. Based on above analysis, it can be summarized that a voltage leap of $V_{ab}$ with the amplitude of $V_{in}/2$ or $-V_{in}/2$ would emerge in the dead time between every two adjacent half cycles.

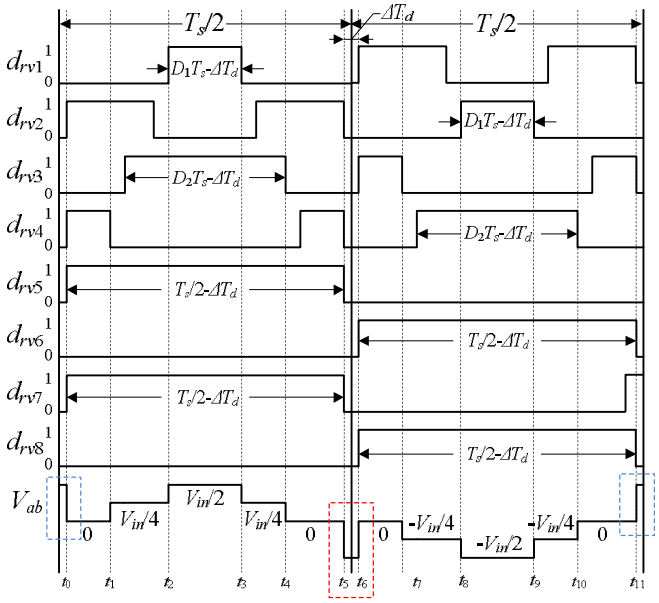


Fig. 3. Operation mode I without $S_9$.

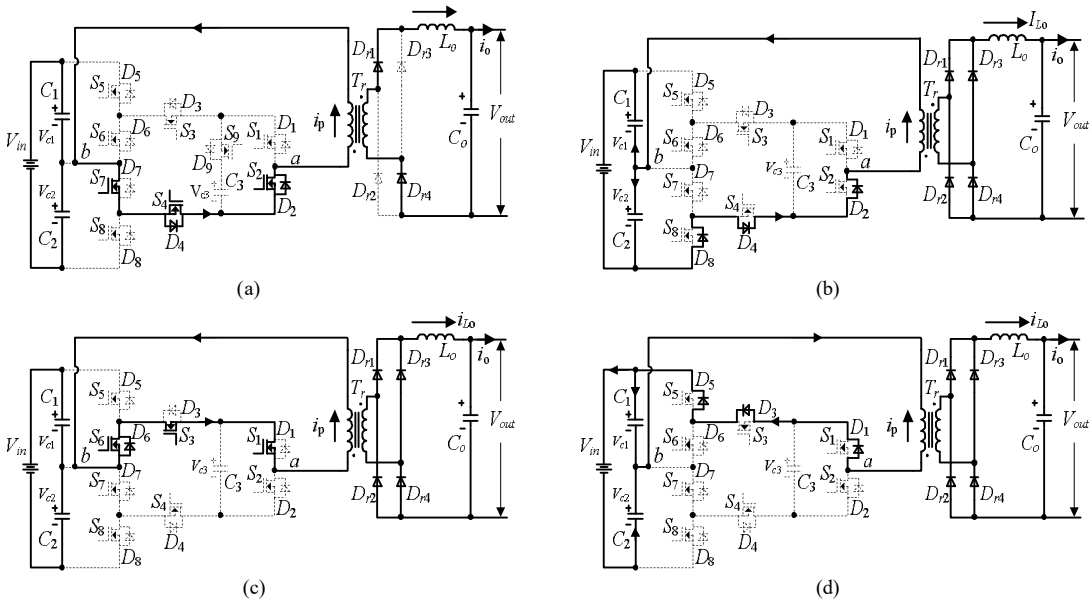


Fig. 4. Equivalent circuits. (a) [$t_4$ - $t_5$]. (b) [$t_5$ - $t_6$]. (c) [$t_6$ - $t_7$]. (d) [$t_{11}$ - $t_0$].

### *B. Proposed Elimination Method for Dead Time Effect*

These voltage leaps need to be eliminated because they have high voltage change rate *dv/dt* resulting in large EMI. Keeping $S_6$ and $S_7$ both on in the dead time can keep $V_{ab}$ at 0 V and get rid of these voltage leaps, however it will short the flying capacitor $C_3$ through $D_3$, $D_4$, $S_6$, and $S_7$ as marked with red color in Fig. 5. In light of this, $S_9$ in series with the flying capacitor $C_3$ is proposed to avoid the short of $C_3$ by switching off $S_9$ when both $S_6$ and $S_7$ are switched on as shown in Fig. 1. Furthermore, after employing $S_9$, the corresponding switching states *V*4 and *V*5 are also proposed to be applied into the proposed modulation strategy as shown in Fig. 2.

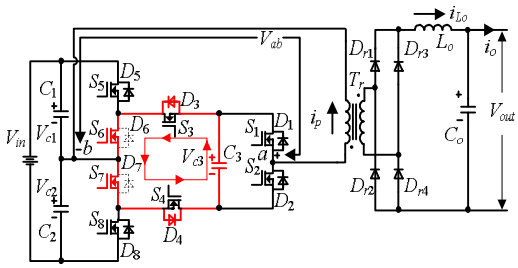

Fig. 5. Short path of $C_3$ without $S_9$.

In the operation mode I, the working principles and equivalent circuits after employing $S_9$ are shown in Fig. 6 and Fig. 7.

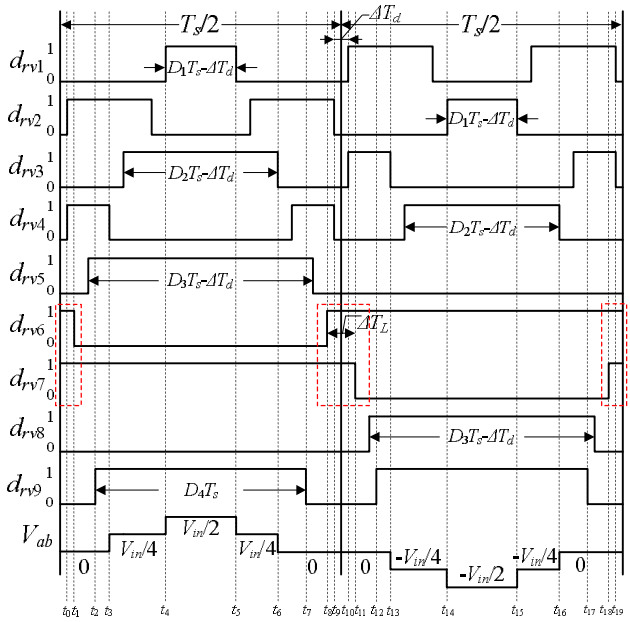


Fig. 6. Operation mode I with $S_9$.

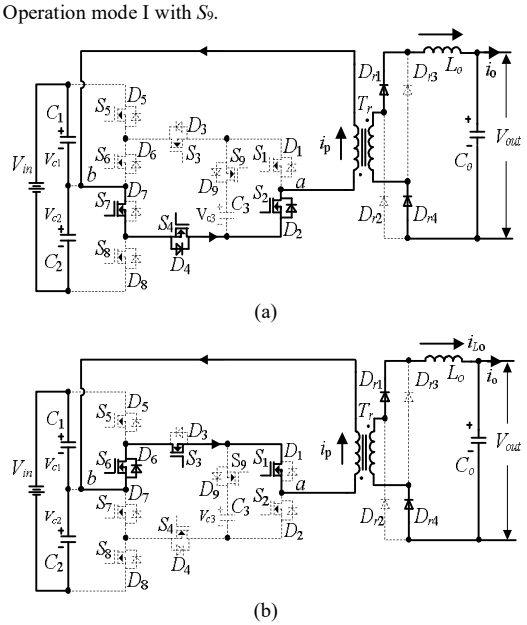


Fig. 7. Equivalent circuits. (a) [$t_7$ - $t_{10}$]. (b) [$t_{10}$ - $t_{12}$].

At $t_7$, $S_9$ is switched off, but this switching action has no effect on $V_{ab}$ since $C_3$ does not involve into the circuit operation at this time. At $t_8$, $S_6$ is switched on, $V_{ab}$ remains at 0V because the $S_2$, $S_4$, and $S_7$ are kept on, shorting the primary side of the transformer. Then, though $S_2$ and $S_4$ are switched off at $t_9$, the primary side of the transformer is still short through $S_7$, $D_2$, and $D_4$ respectively. At $t_{10}$, $S_1$ and $S_3$ are switched on, thus the on-state of $S_1$, $S_3$, and $S_6$ keep $V_{ab}$ at 0 V. Finally, $S_7$ and $S_9$ are switched off at $t_{11}$ and $t_{12}$ respectively, but making no influence on $V_{ab}$. From the above analysis, $V_{ab}$ stays at 0V in the period [$t_7$, $t_{12}$]. The equivalent circuits in period [$t_7$, $t_{10}$] and [$t_{10}$, $t_{12}$] are shown in Fig. 7(a) and Fig. 7(b) respectively. At $t_{17}$, $S_9$ is switched off for the next half cycle. The following operation works similarly to that in period [$t_7$, $t_{12}$] and $V_{ab}$ also maintains at 0 V. One thing to be mentioned is that the duty ratios $D_3$ and $D_4$ are set for eliminating the dead time effect, in which $D_3$ is set shorter than 0.5 to gain overlap time $\Delta T_L$ between two switching functions of $S_6$ and $S_7$ in every half cycle as marked in Fig. 6. The overlap time $\Delta T_L$ needs to be longer than dead time $\Delta T_d$ and $D_4$ is required to be shorter than ($D_3$-$\Delta T_d/T_s$). Based on the above analysis, the employed $S_9$ only has switching actions when $V_{ab}$ equals to 0 V. Furthermore, the switching actions of $S_9$ happen while there is no current flowing through $S_9$ and have no effect on the $V_{ab}$ and $i_p$. The voltages on $S_1$, $S_2$, $S_3$, and $S_4$ could not clamped by the flying capacitor $C_3$ when $S_9$ is turned off in the dead time, but increasing the capacitance of the paralleled capacitors of the switches $S_3$ and $S_4$ can make the voltages on $C_1$, $C_3$ and voltages on $C_2$, $C_4$ are balanced. Therefore, the proposed elimination method of the dead time effect by employing $S_9$ in series with the flying capacitor $C_3$ would not cause voltage unbalance among the power switches $S_1$, $S_2$, $S_3$, and $S_4$ in the dead time for the high power applications. In addition, from Fig. 6 it can be observed that: 1) $S_5$-$S_8$ and $S_9$ can achieve zero-current-switching; 2) $S_1$-$S_4$ can achieve zero-voltage switch-on in most switching operations except that $S_1$ cannot achieve zero-voltage switch-on at $t_4$; $S_2$ cannot achieve zero-voltage switch-on at $t_{14}$.

In summary, after using the proposed elimination method for the dead time effect, $V_{ab}$ can be kept at 0 V in the dead time between every two adjacent half cycles in the operation mode I, which avoids causing high voltage leaps. The dead time effect in the operation mode II can also be eliminated with the same method utilized in the operation mode I, which is not repeated here.

## IV. Proposed Capacitor Voltage Control Strategy

The voltage balance of the flying capacitor $C_3$ is one of the important issues in the proposed converter because it directly affects multi-level voltage waveforms. In this section, a capacitor voltage control strategy is proposed.

### A. In Operation Mode I

From Fig. 2 (a), in the first half cycle, it can be observed that $V_{ab}$ is positive and the switching states are:

$$V4 \rightarrow V3 \rightarrow V2 \rightarrow V0 \rightarrow V2 \rightarrow V3 \rightarrow V4 \quad (1)$$

According to Fig. 2 and Table I, the charge or discharge of the flying capacitor $C_3$ occurs when $V_{ab}$ equals $V_{in}/4$ or -$V_{in}/4$, and the related switching states are $V1$, $V2$, $V7$, or $V8$. Furthermore, $C_3$ is charged in switching states $V2$, $V7$ and is discharged in $V1$, $V8$ respectively. In the first half cycle, the switching state is $V2$ when $V_{ab}$ equals $V_{in}/4$. Therefore, $C_3$ is charged in the first half cycle according to the above analysis.

In the second half cycle, $V_{ab}$ is negative and the switching states are:

$$V5 \rightarrow V6 \rightarrow V7 \rightarrow V9 \rightarrow V7 \rightarrow V6 \rightarrow V5 \quad (2)$$

Similar to the analysis of the first half cycle, the switching state is $V7$ when $V_{ab}$ equals -$V_{in}/4$ in the second half cycle, so $C_3$ is also charged and not discharged in the second half cycle. In summary, $C_3$ is charged but not discharged in the operation mode I.

### B. In Operation Mode II

From Fig. 2 (b), in the first half cycle, $V_{ab}$ is positive and the

switching states are:

$$V4 \rightarrow V3 \rightarrow V1 \rightarrow V0 \rightarrow V1 \rightarrow V3 \rightarrow V4 \quad (3)$$

In the second half cycle, $V_{ab}$ is negative and the switching states are:

$$V5 \rightarrow V6 \rightarrow V8 \rightarrow V9 \rightarrow V8 \rightarrow V6 \rightarrow V5 \quad (4)$$

With the similar analysis as the operation mode I that the charge or discharge situation of $C_3$ occurs when $V_{ab}$ equals $V_{in}/4$ or $-V_{in}/4$, it can be observed that the switching states are $V1$ and $V8$ respectively when $V_{ab}$ equals to $V_{in}/4$ and $-V_{in}/4$. Therefore, $C_3$ is discharged but not charged in the operation mode II.

### C. *Proposed Capacitor Voltage Control Strategy*

According to above analysis, the voltage of the flying capacitor $C_3$ would increase in the operation mode I and decrease in the operation mode II as shown in Fig. 2. Consequently, a capacitor voltage control strategy is proposed for balancing $V_{c3}$ by alternatively utilizing the two operation modes of the proposed modulation strategy as shown in Fig. 8, in which a comparator is used with two input voltages $V_{c3}$ and $V_{ref\_c3}$. $V_{ref\_c3}$ is a voltage reference of the flying capacitor $C_3$ and is normally set at a quarter of input voltage $V_{in}/4$. If $V_{c3}$ is less than $V_{ref\_c3}$, the operation mode I is selected for the next cycle. Otherwise, the operation mode II is chosen for the next cycle when $V_{c3}$ is more than or equals to $V_{ref\_c3}$.

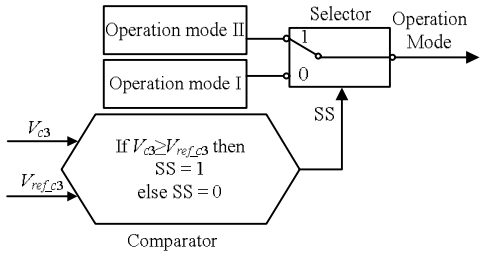


Fig. 8. Diagram of the proposed capacitor voltage control strategy.

## V. Simulation And Experimental Verification

### A. *Simulation Verification*

In the simulation model, a case which applies the proposed converter to transfer power from the dc bus voltage with 4 kV to the dc loads with the input voltages (800 V) is studied. The parameters of the simulation model are listed in Table II. When the proposed converter operates at a steady state, simulation results are shown in Fig. 9, which includes voltages $V_{in}$, $V_{ab}$, $V_{c3}$, $V_{out}$ and currents $i_p$, $i_o$.

In Fig. 9, it can be observed that the five-level voltages are produced on the primary side of the transformer by the proposed modulation strategy, which effectively reduces the voltage change rate *dv/dt*, and the voltage of the flying capacitor $V_{c3}$ can be controlled at 1 kV constantly by utilizing the proposed capacitor voltage control strategy.

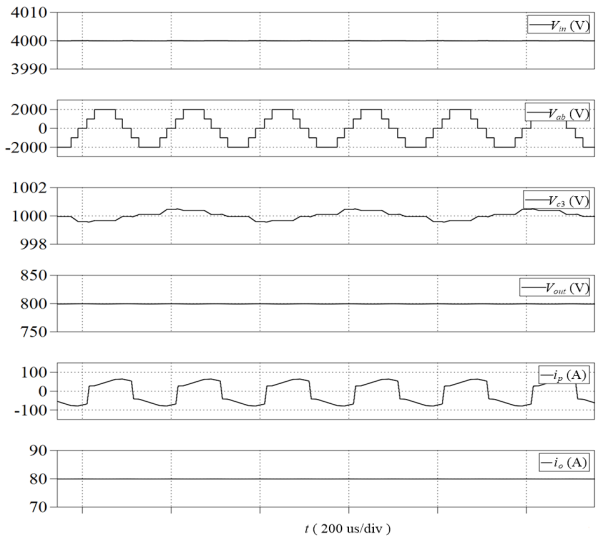


Fig. 9. Simulation results including $V_{in}$, $V_{ab}$, $V_{c3}$, $V_{out}$, $i_p$, and $i_o$.

Through comparing results between without $S_9$ and with $S_9$ as exhibited in Fig. 10, it can be observed that the high voltage leaps caused by the dead time effect are effectively eliminated after utilizing the proposed elimination method.

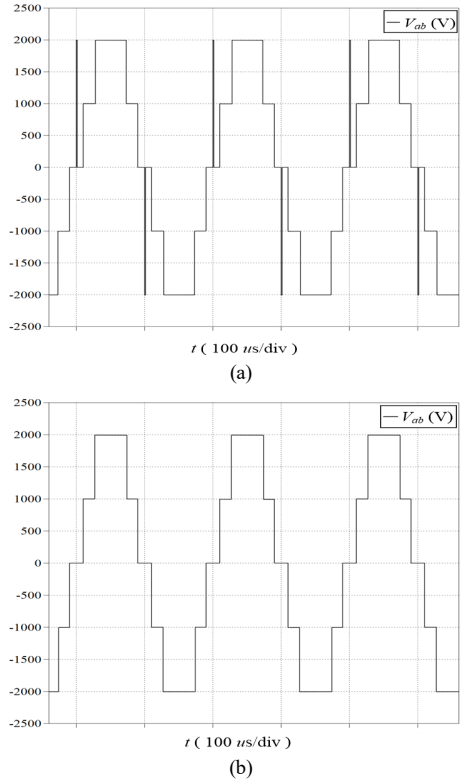


Fig. 10. Simulation results of $V_{ab}$. (a) Without $S_9$. (b) With $S_9$.

According to the circuit parameters and simulation results of the simulation model, the efficiency by theoretical calculation [44] under the full load (64-kW) is about 94.8%, in which the parameters of FS100R17N3E4 and FF200R33KF2C are used for $S_1/D_1$-$S_4/D_4$, $S_9/D_9$ and $S_5/D_5$-$S_8/D_8$ respectively and the parameters of DDB6U144N16 are used for the output rectifier diodes. Fig. 11 presents the theoretically calculated distribution of the power losses under the full load.

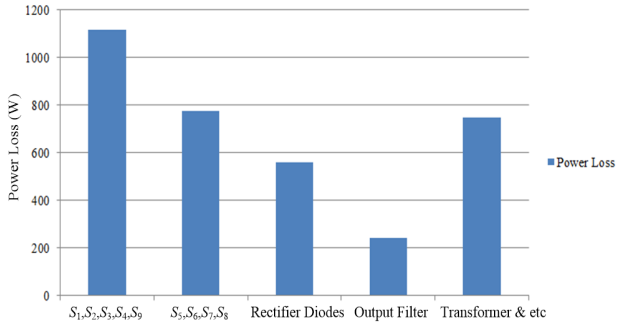


Fig. 11. Caculated power loss distribution under 64-kW ($D_2$ = 0.35).

## B. Experimental Verification

In order to verify the performances of the proposed converter and voltage control strategy, a 1-kW laboratory prototype is built and tested. A simple PI controller is applied in the prototype to control the output voltage. The parameters of the experimental setup are listed in Table III.

The performances of the proposed converter operating at 250 W are shown in Figs. 12-14, in which (a) is with $D_2$ = 0.35, and (b) is with $D_2$ = 0.3. Fig. 12(a) and Fig. 12(b) show $V_{ab}$, $V_{c3}$, $i_{Lo}$, and $i_p$. It can be seen that the five-level voltages are produced on the primary side voltage of transformer $V_{ab}$, which can effectively reduce the voltage change rate *dv/dt*, and the voltage of the flying capacitor $V_{c3}$ is controlled constantly at about 60 V by the proposed capacitor voltage control strategy. The voltages of $C_1$ and $C_2$ are about 120 V which is half of input voltage as shown in Fig. 13(a) and Fig. 13(b). In Fig. 14(a) and Fig. 14(b), $V_{out}$, $i_o$, and $V_{ds\_S9}$ are exhibited. $V_{ds\_S9}$ is the drain-source voltage of $S_9$. It can be seen that the voltage stress of $S_9$ is only about 60 V, which is a quarter of the input voltage, and $V_{out}$ is controlled at 100 V constantly.

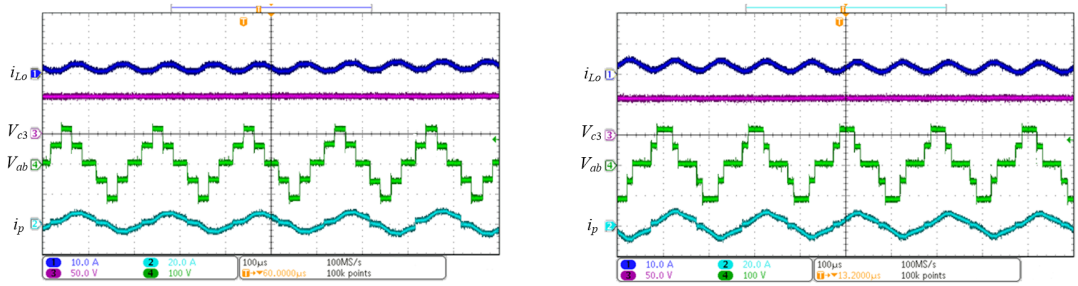


(a) (b)

Fig. 12. Experimental results under 250 W including $i_{Lo}$, $V_{ab}$, $V_{c3}$, and $i_p$. (a) $D_2$ = 0.35. (b) $D_2$ = 0.3.

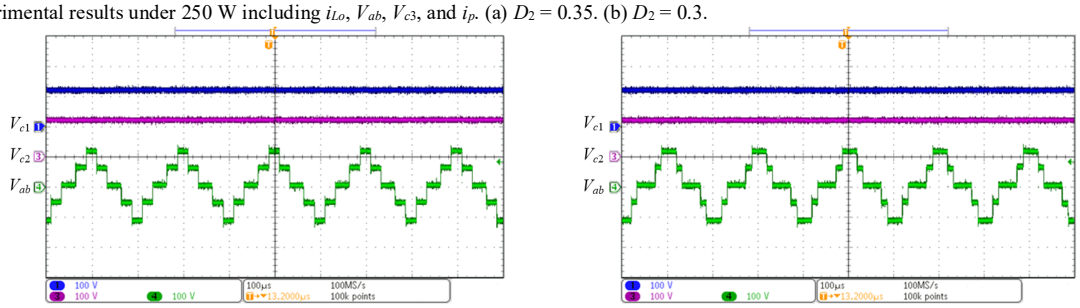


(a) (b)

Fig. 13. Experimental results under 250 W including $V_{c1}$, $V_{c2}$, and $V_{ab}$. (a) $D_2$ = 0.35. (b) $D_2$ = 0.3.

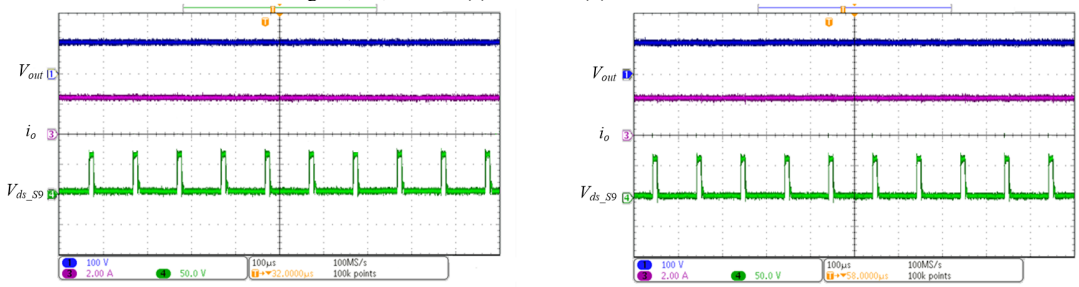


(a) (b)

Fig. 14. Experimental results under 250 W including $V_{out}$, $i_o$, and $V_{ds\_S9}$. (a) $D_2$ = 0.35. (b) $D_2$ = 0.3.

Figs. 15-17 show the performances of the proposed converter operating at 500 W, in which (a) is with $D_2$ = 0.35, and (b) is with $D_2$ = 0.3 respectively. $V_{ab}$, $V_{c3}$, $i_{Lo}$, and $i_p$ are shown in Fig. 15(a) and Fig. 15(b). It is can be seen that $V_{ab}$ has five-level voltages and $V_{c3}$ is also kept at about 60 V. Fig. 16(a) and Fig. 16(b) show the votlage of $C_1$ and $C_2$, which are about 120 V. In Fig. 17(a) and Fig. 17(b), $V_{out}$, $i_o$, and $V_{ds\_S9}$ are shown and $S_9$ only sustains about 60 V which is a quarter of the input voltage.

Based on the above experimental results, it can be observed that five-level voltages are generated on the transformer, which

can reduce the voltage change rate *dv*/*dt*, voltage stress and harmonics on the transformer. Such advantages can not only improve the reliability of the transformer but also improve the reliability of the converter by reducing the EMI.

The comparison results between with $S_9$ and without $S_9$ are shown in Fig. 18. The voltage leaps of $V_{ab}$ between every two adjacent half cycles caused by the dead time are effectively eliminated by utilizing the proposed elimination method.

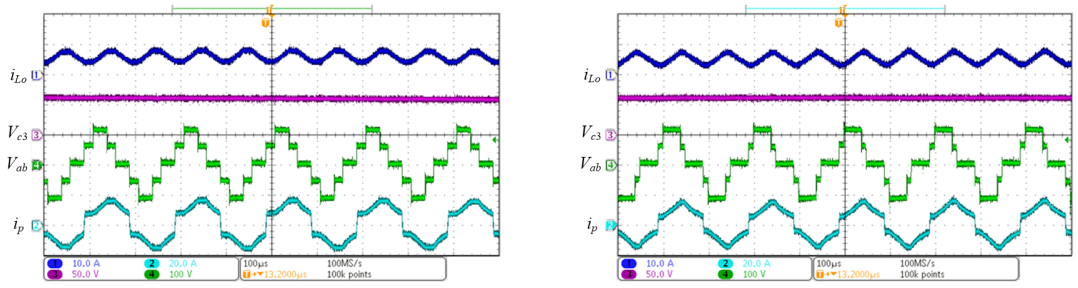


Fig. 15. Experimental results under 500 W including $i_{Lo}$, $V_{ab}$, $V_{C3}$, and $i_p$. (a) $D_2 = 0.35$. (b) $D_2 = 0.3$.

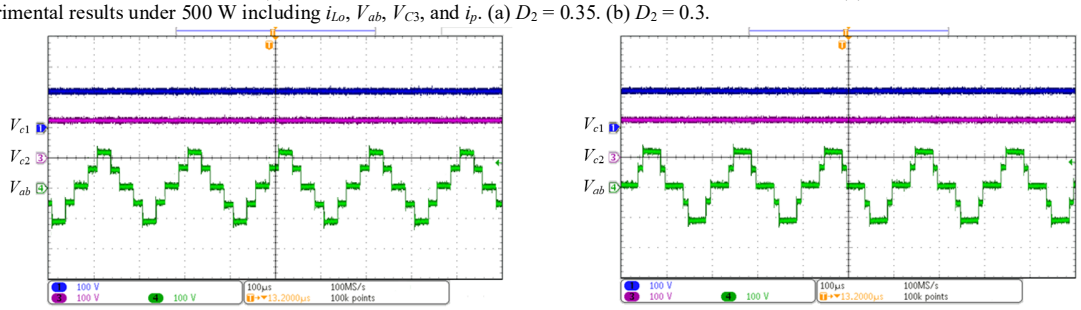


Fig. 16. Experimental results under 500 W including $V_{c1}$, $V_{c2}$, and $V_{ab}$. (a) $D_2 = 0.35$. (b) $D_2 = 0.3$.

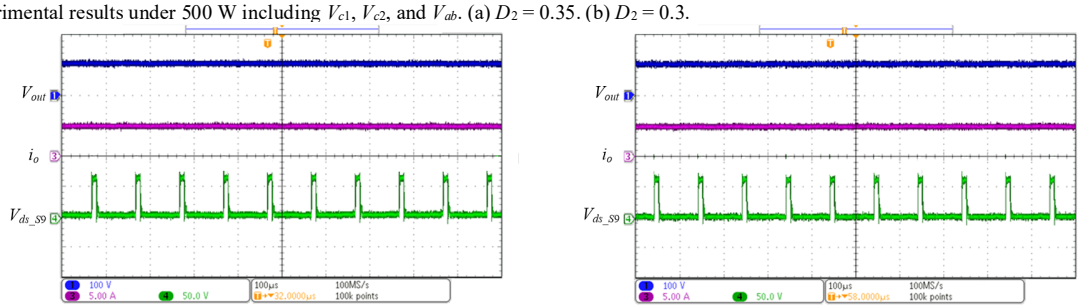


Fig. 17. Experimental results under 500 W including $V_{out}$, $i_o$, and $V_{ds\ S9}$. (a) $D_2 = 0.35$. (b) $D_2 = 0.3$.

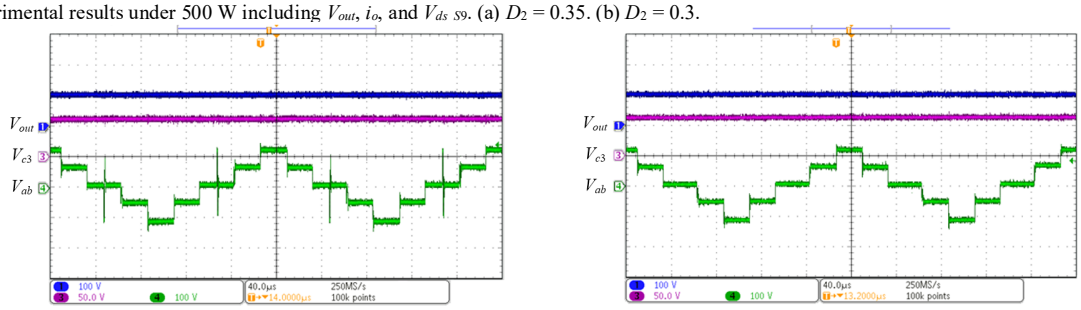


Fig. 18. Comparison result under 250 W including $V_{out}$, $V_{c3}$, and $V_{ab}$ ($D_2 = 0.35$). (a) Without $S_9$. (b) With $S_9$.

Fig. 19 and Fig. 20 show the dynamic performances of the proposed converter. In Fig. 19(a), the output voltage reference $V_{ref\_Vo}$ changes from 100 V to 80 V and finally gets back to 100 V. The details about zone 1 and zone 2 in Fig. 19(a) are shown in Fig. 19(b) and Fig. 19(c) respectively. Fig. 20 exhibits the performance under the load changes, in which the load changs from 40 Ω to 20 Ω and finally sets back to 40 Ω. In summary, the voltage of the flying capacitor $V_{c3}$ is controlled constantly without significant changes under the dynamic tests.

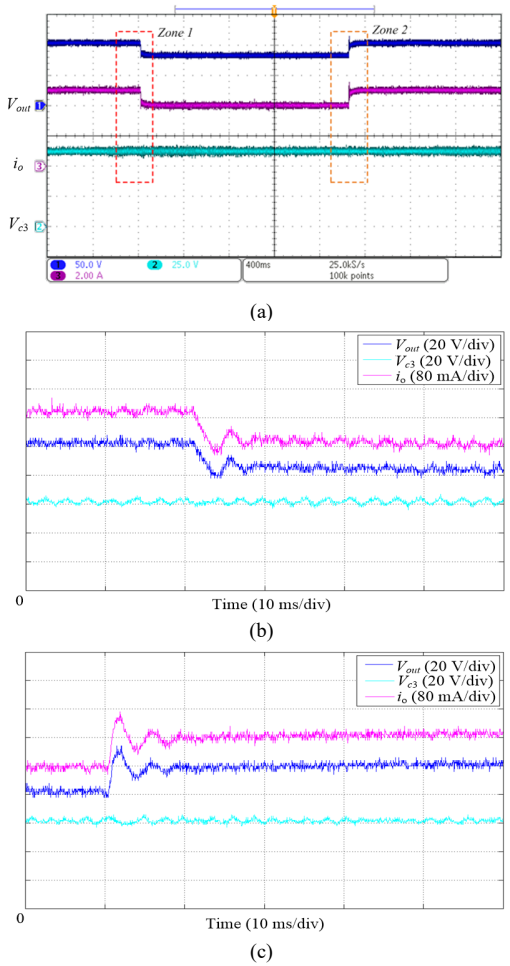


Fig. 19. Dynamic performance ($D_2$ = 0.35). (a) Output voltage reference changes. (b) Zone 1. (c) Zone 2.

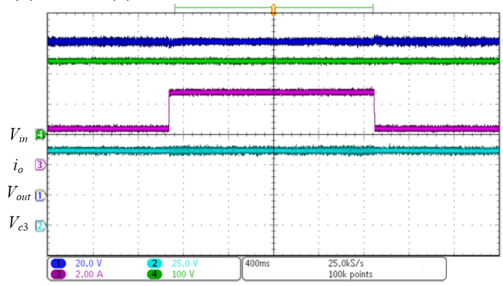


Fig. 20. Dynamic performance under load changes ($D_2$ = 0.35).

Fig. 21 shows the efficiency curves of the proposed converter under the power variations, in which one is with $D_2$ = 0.35, and the other one is with $D_2$ = 0.3. The average deviation between the two efficiency curves is about 0.2%.

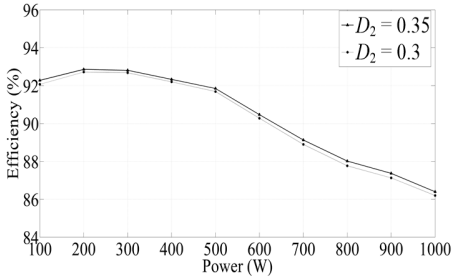


Fig. 21. Efficiency results with $D_2$ = 0.35 and $D_2$ = 0.3 under the power variations.

Fig. 22 illustrates the distribution of the power losses in the experimental prototype when $D_2$ is 0.35 and the output power is 1-kW. It can be obersved that: 1) the switching loss of the power swithes is small because the switching frequency is low (5 kHz) and the power switches can achieve zero-voltage switching or zero-current switching in the most operations; 2) the dominant part of the power losses is the conduction loss of the power switches since the voltage conversion ratio between the input voltage and output voltage in the prototype is small, which means that the primary current is higher. In the full-scale converter like the simulation model, the voltage conversion ratio is high, so the efficiency will increase siginificantly arising from the decreasing conduction loss of the power switches.

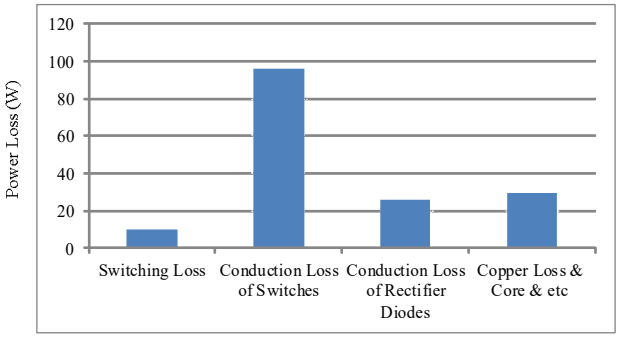


Fig. 22. Power loss distribution under 1-kW ($D_2$ = 0.35).

## VI. Conclusion

This paper has proposed a 5L-ANPC dc/dc converter with a corresponding modulation strategy for the applications in MVDC grids. Due to multi-level voltages generating, the proposed converter can effectively reduce the voltage change rate *dv/dt* and the voltage stress on the transformer, thus reduce EMI and increase system reliability. An elimination method for the dead time effect is proposed by employing a switch in series with the flying capacitor, which can eliminate high voltage leaps caused by the dead time effect. In addition, a capacitor voltage control strategy by alternatively utilizing the two operation modes of the proposed modulation strategy is proposed for balancing the voltage of the flying capacitor, which can ensure the generation of the desired multi-level voltage waveforms. Finally, a simulation model and a down-scale laboratory prototype of the proposed converter have been built. The simulation and experimental results are in line with the theoretical analysis, which validates the feasibility of the proposed converter and voltage control strategy. It is highly recommended that the bidirectional dc/dc converter will be taken into consideration in the future studies, considering that more bidirectional power flows from new smart grid elements (e.g. energy storage system and electric vehicles) emerge in DC grids.

## Appendix

See Table II and III.

TABLE II
PARAMETERS OF THE SIMULATION MODEL

| Components | Description |
|---|---|

| | |
|---|---|
| Turns Ratio of Transformer | 2:1 |
| Output Filter Capacitor $C_o$ ($uF$) | 1500 |
| Output Filter Inductor $L_o$ ($mH$) | 1 |
| Input Capacitors $C_1$ and $C_2$ ($uF$) | 6800 |
| Flying Capacitor $C_3$ ($uF$) | 3500 |
| Input Voltage $V_{in}$ ($kV$) | 4 |
| Output Voltage Reference $V_{ref\_Vo}$ ($V$) | 800 |
| Voltage Reference of Flying Capacitor $V_{ref\_c3}$ ($kV$) | 1 |
| Switching Frequency ($kHz$) | 5 |
| Load $R_o$ ($\Omega$) | 10 |
| Dead Time ($us$) | 1 |

TABLE III
PARAMETERS OF THE EXPERIMENTAL SETUP

| Components | Description |
|---|---|
| Mosfets $S_1/D_1$-$S_4/D_4$, $S_9/D_9$ | IRFP4137PBF |
| Mosfets $S_5/D_5$-$S_8/D_8$ | SPW47N60C3 |
| Rectifier Diodes $D_{r1}$-$D_{r4}$ | FFA60UP30DNTU |
| Turns Ratio of Transformer | 1:2 |
| Output Filter Capacitor $C_o$ ($uF$) | 470 |
| Output Filter Inductor $L_o$ ($mH$) | 1 |
| Input Capacitors $C_1$ and $C_2$ ($uF$) | 1500 |
| Flying Capacitor $C_3$ ($uF$) | 1500 |
| Input Voltage $V_{in}$ ($V$) | 240 |
| Output Reference Voltage $V_{ref\_Vo}$ ($V$) | 100 |
| Voltage Reference of Flying Capacitor $V_{ref\_c3}$ ($V$) | 60 |
| Switching Frequency ($kHz$) | 5 |
| Dead Time ($us$) | 1.5 |

## REFERENCES


[1] R. S. Balog, W. Weaver, and P. T. Krein, "The Load as an Energy Asset in a Distributed DC Smart Grid Architecture," *IEEE Trans. Smart Grid*., vol. 3, no. 1, pp. 253–260, Mar. 2012.

[2] H. Mohsenian-Rad, and A. Davoudi, "Towards Building an Optimal Demand Response Framework for DC Distribution Networks," *IEEE Trans. Smart Grid*., vol. 5, no. 5, pp. 2626-2634, Sep. 2014.

[3] G. F. Reed, B. M. Grainger, A. R. Sparacino, and M. Zhi-Hong, "Ship to grid: Medium-voltage DC concepts in theory and practice," *IEEE Power Energy Mag.,* vol. 10, no. 6, pp. 70–79, Nov. 2012.

[4] S.Anand andB. G.Fernandes, "Optimal voltage level for DC microgrids," in *Proc. IEEE Conf. Ind. Electron.,* 2010, pp. 3034–3039.

[5] D. Salomonsson, L. Soder, and A. Sannino, "An adaptive control system for a DC microgrid for data centers," *IEEE Trans. Ind. Appl.,* vol. 44, no. 6, pp. 1910–1917, Nov./Dec. 2008.

[6] W. Chen, A. Q. Huang, C. Li, G. Wang, and W. Gu, "Analysis and comparison of medium voltage high power DC/DC converters for offshore wind energy systems," *IEEE Trans. Power Electron*., vol. 28, no. 4, pp. 2014– 2023, Apr. 2013.

[7] H. Wu, K. S. Ding, and Y. Xing, "Topology derivation of nonisolated three-port DC–DC converters from DIC and DOC," *IEEE Trans. Power Electron*., vol. 28, no. 7, pp. 3297–3307, Jul. 2013.

[8] W. Chen et al., "A comparison of medium voltage high power dc/dc converters with high step-up conversion ratio for offshore wind energy systems," in *Proc. IEEE ECCE.,* 2011, pp. 584–589.

[9] F. Blaabjerg, Z. Chen, and B. S. Kjaer, "Power electronics as efficient interface in dispersed power generation systems," *IEEE Trans. Power Electron*., vol. 19, no. 5, pp. 1184–1194, Sep. 2004.

[10] Y. Matsuoka, M. Nakahara K. Wada, K. Takao, K. Sung, and S. Nishizawa, "2.5kV, 200kW Bi-Directional Isolated DC/DC Converter for Medium-Voltage Applications," *in Proc. IEEE Conf. ECCE-Asia*, 2014, pp. 744-749.

[11] D.Vinnikov, T. Jalakas, and M.Egorov, "Feasibility study of half- and full-bridge isolated DC/DC converters in high-voltage high-power applications," in *Proc. 13th EPE-PEMC.,* Sep. 2008, pp.1257-1262.

[12] L. Max and S. Lundberg, "System efficiency of a DC/DC converter based wind farm," *Wind Energy*., vol. 11, pp. 109–120, Oct. 2008.

[13] G. Ortiz, J. Biela, D. Bortis, and J. Kolar, "1 Megawatt, 20 kHz, isolated, bidirectional 12kV to 1.2kV dc–dc converter for renewable energy applications," in *Proc. IPEC*., Jun. 2010, pp. 3212–3219.

[14] F. Blaabjerg, F. Iov, Z. Chen, and K. Ma, "Power electronics and controls for wind turbine systems," in *Proc. IEEE Int. Energy Conf. Exhib*., Dec. 2010, pp. 333–344.

[15] N. Mohan, T. M. Undeland, and W. P. Robbins, *Power Electronics: Converters, Applications, and Design*, 3rd ed. New York: Wiley, 2003.

[16] N. Y. Dai, M. C.Wong, and Y. D. Han, "Application of a three-level NPC inverter as a three-phase four-wire power quality compensator by generalized 3DSVM," *IEEE Trans. Power Electron*., vol. 21, no. 2, pp. 440–449, Mar. 2006.

[17] S. Kenzelmann, A. Rufer, M. Vasiladiotis, D. Dujic, F. Canales, and Y. R. de Novaes, "A versatile dc–dc converter for energy collection and distribution using the modular multilevel converter," in *Proc. 14th Eur. Conf. Power Electron. Appl*., Aug./Sep. 2011, pp. 1–10.

[18] J. A. Ferreira, "The multilevel modular DC converter," *IEEE Trans. Power Electron*., vol. 28, no. *10*, Oct. 2013.

[19] R. Mo, R. Li, and H. Li, "Isolated modular multilevel (IMM) DC/DC converter with energy storage and active filter function for shipboard MVDC system applications" in *Proc. IEEE ESTS.*, 2015, pp. 113-117.

[20] H. Nademi, A. Das, and L. Norum, "Modular multilevel converter with adaptive observer of capacitor voltages," *IEEE Trans. Power Electron*., vol. 30, no. 1, pp. 235–248, Jan. 2014.

[21] S. Debnath, J. Qin, B. Bahrani, M. Saeedifard, and P. Barbosa, "Operation, control, and applications of the modular multilevel converter: A review," *IEEE Trans. Power Electron*., vol. 30, no. 1, pp. 37–53, Jan. 2015.

[22] F. Deng and Z. Chen, "A control method for voltage balancing in modular multilevel converters," *IEEE Trans. Power Electron*., vol. 29, no. 1, pp. 66–76, Jan. 2014.

[23] T. Luth, M. Merlin, T. Green, F. Hassan, and C. Barker, "High-frequency operation of a DC/AC/DC system for HVDC applications," *IEEE Trans. Power Electron*., vol. 29, no. 8, pp. 4107–4115, Aug. 2014.

[24] G. J. Kish, M. Ranjram, and P. W. Lehn, "A modular multilevel dc/dc converter with fault blocking capability for HVDC interconnects," *IEEE Trans. Power Electron*., vol. 30, no. 1, pp. 148–162, Jan. 2015.

[25] X.Ruan, B. Li,Q. Chen, S. C. Tan, and C.K. Tse, "Fundamental considerations of three-level dc-dc converters: Topologies, analyses, and control," *IEEE Trans. Circuits Syst. I, Reg. Papers*., vol. 55, no. 11, pp. 3733–3743, Dec. 2008.

[26] J. R. Pinheiro and I. Barbi, "The three-level ZVS PWM converter—a new concept in high-voltage DC-to-DC conversion," in *Proc. IEEE Int. Conf. Ind. Electron. Control Instrum. Autom*., 1992, pp. 173–178.

[27] F. Canales, P. Barbosa, and F. C. Lee, "A zero-voltage and zero-current switching three-level dc/dc converter," *IEEE Trans. Power Electron*., vol. 17, no. 6, pp. 898–904, Nov. 2002.

[28] R. Xinbo, L. Zhou, and Y. Yan, "Soft-switching PWM three-level converters," *IEEE Trans. Power Electron*., vol. 16, no. 5, pp. 612–622, Sep. 2001.

[29] Z. Zhang and X. Ruan, "Zero-Voltage-Switching PWM full-bridge three-level converter," in *Proc. 4th Int. Power Electron. Motion Control Conf*., 2004, pp. 1085–1090.

[30] X. Ruan, Z. Chen, and W. Chen, "Zero-voltage-switching PWM hybrid full-bridge three-level converter," *IEEE Trans. Power Electron*., vol. 20, no. 2, pp. 395–404, Mar. 2005.

[31] I.-O. Lee and G.-W. Moon, "Analysis and design of a three-level LLC series resonant converter for high- and wide-input-voltage applications," *IEEE Trans. Power Electron*., vol. 27, no. 6, pp. 2966–2979, Jun. 2012.

[32] B. R. Lin and C. H. Liu, "ZVS DC/DC converter based on two three-level PWM circuits sharing the same power switches," *IEEE Trans. Power Electron*., vol. 60, no. 10, pp. 4191–4200, Oct. 2013.

[33] D.-Y. Kim, J.-K. Kim, and G.-W Moon, "A three-level converter with reduced filter size using two transformers and flying capacitors," *IEEE Trans. Power Electron*., vol. 28, no. 1, pp. 46–53, Jan. 2013.

[34] Y. Shi and X. Yang, "Wide range soft switching PWM three-level DCDC converters suitable for industrial applications," *IEEE Trans. Power Electron*., vol. 29, no. 2, pp. 603–616, Feb. 2014.

[35] F. Deng and Z. Chen, "Control of improved full-bridge three-level DC/DC converter for wind turbines in a DC grid," *IEEE Trans. Power Electron*., vol. 28, no. 1, pp. 314–324, Jan. 2013.

[36] Y. Chen, M. Haj-ahmed, and M. S. Illindala, "An MVDC microgrid for a remote area mine site: Protection, operation and control," in *Proc. IEEE IAS Annu. Meet*., Oct. 2014, pp. 1–9.

[37] B. M. Grainger, A. R. Sparacino, R. J. Kerestes, and M. J. Korytowski, "Advancements in medium voltage DC architecture development with applications for powering electric vehicle charging stations," in *Energytech, 2012 IEEE*, 2012, pp. 1–8.

[38] M. Saeedifard, M. Graovac, R. F. Dias, and R. Iravani, "DC power systems: Challenges and opportunities," in *Proc. IEEE Power Energy Soc. Gen. Meet*., 2010, pp. 1–7.
[39] M. Baran and N. R Mahajan, "DC distribution for industrial systems opportunities and challenges," *IEEE Trans. Ind. Appl*., vol. 39, no. 6, pp. 1596–1601, Nov./Dec. 2003.
[40] P. Karlsson and J. Svensson, "Dc bus voltage control for a distributed power system," *IEEE Trans. Power Electron*., vol. 18, no. 6, pp. 1405–1412, Nov. 2003.
[41] T. Hakala, T. Lähdeaho, and P. Järventausta, "Low-voltage DC distribution—utilization potential in a large distribution network company," *IEEE Trans. Power Del*., vol. 30, no. 4, pp. 1694–1701, Aug. 2015.
[42] P. Barbosa, P. Steimer, J. Steinke, L. Meysenc, M. Winkelnkemper, and N. Celanovic, "Active-neutral-point-clamped multilevel converters," *in Proc. IEEE 36th Power Electron. Spec. Conf*., Jun. 16, 2005, pp. 2296–230.
[43] S. R. Pulikanti and V. G. Agelidis, "Hybrid flying-capacitor-based active-neutral-point-clamped five-level converter operated with SHE-PWM," *IEEE Trans. Ind. Electron*., vol. 58, no. 10, pp. 4643–4653, Oct. 2011.
[44] D. Graovac, M. Purschel. (2009 , Jan . ). IGBT power losses calculation using the data-sheet parameters: Application note. Infineon Corp., Germany. [Online]. Available: http://www.infineon.com/

**Dong Liu** (**S**'2015) received the B.Eng. degree and M.Sc. degree in electrical engineering from South China University of Technology, Guangdong, China, in 2008 and 2011 respectively. From 2011 to 2014, he was a R&D Engineer in Emerson Network Power Co., Ltd., China.

He is currently working toward the Ph.D. degree in the Department of Energy Technology, Aalborg University, Denmark.

His main research interests include renewable energy, multilevel converters, DC grid, and dc/dc converters.

**Fujin Deng** (**S**'10-**M**'13) received the B.Eng. degree in electrical engineering from China University of Mining and Technology, Jiangsu, China, in 2005, the M.Sc. Degree in electrical engineering from Shanghai Jiao Tong University, Shanghai, China, in 2008, and the Ph.D. degree in energy technology from the Department of Energy Technology, Aalborg University, Aalborg, Denmark, in 2012.

From 2013 to 2015, he was a Postdoctoral Researcher in the Department of Energy Technology, Aalborg University, Aalborg, Denmark. Currently, he is an Assistant Professor in the Department of Energy Technology, Aalborg University, Aalborg, Denmark. His main research interests include wind power generation, multilevel converters, DC grid, high-voltage direct-current (HVDC) technology, and offshore wind farm-power systems dynamics.

**Zhe Chen** (M'95–SM'98) received the B.Eng. and M.Sc. degrees all in Electrical Engineering from Northeast China Institute of Electric Power Engineering, Jilin City, China, MPhil in Power Electronic, from Staffordshire University, England and the Ph.D. degree in Power and Control, from University of Durham, England.

Dr Chen is a full Professor with the Department of Energy Technology, Aalborg University, Denmark. He is the leader of Wind Power System Research program at the Department of Energy Technology, Aalborg University and the Danish Principle Investigator for *Wind Energy* of *Sino-Danish Centre for Education and Research*.

His research areas are power systems, power electronics and electric machines; and his main current research interests are wind energy and modern power systems. He has led many research projects and has more than 400 technical publications with more than 10000 citations and h-index of 44 (Google Scholar).

Dr Chen is an Associate Editor of the IEEE Transactions on Power Electronics, a Fellow of the Institution of Engineering and Technology (London, U.K.), and a Chartered Engineer in the U.K.